Passive Intermodulation Generation on Printed Lines: Near-Field Probing and Observations

Aleksey P. Shitvov, Dmitry E. Zelenchuk, *Member, IEEE*, Alexander G. Schuchinsky, *Senior Member, IEEE*, and Vincent F. Fusco, *Fellow, IEEE*

***Abstract*—The phenomenological mechanisms of passive intermodulation (PIM) in printed lines have been explored by mapping intermodulation products generated by the two-tone traveling waves in microstrip lines. Near-field probing based upon a commercial PIM analyzer has been employed for identification of the PIM sources in printed lines. The results of extensive near-field probing provide the direct experimental evidences of cumulative growth of the intermodulation products in the matched uniform microstrip lines and reveal the fundamental role of the nonlinear scattering by the lumped nonlinear inclusions in the intermodulation production. The distributed nature of the PIM generation in microstrip lines has been conclusively demonstrated and comprehensively described in terms of the four-wave mixing process that proved to be fully consistent with the results of experimental observations of third-order PIM products on the matched and mismatched microstrip lines.**

***Index Terms*—Four-wave mixing, near-field probing, passive intermodulation (PIM), printed circuit board (PCB) material characterization, printed circuits.**

I. Introduction

PASSIVE intermodulation (PIM) manifests itself as spurious signals degrading performance of communication systems. It was originally observed as the products of nonlinear mixing at contacts of dissimilar metals, dry joints, spot corrosion (rusty bolts), etc. [1], [2]. In contrast to PIM sources in waveguide junctions and cable joints [3], duplexers [4], attenuators [5], and antennas [6], where they have been extensively studied [1], [3]–[5], [7]–[9], the physical mechanisms of PIM generation in printed circuit boards (PCBs) are still barely understood.

PCBs constitute a key element of the communication equipment. The range of PCB applications extends from the basic interconnects to sophisticated beam-forming networks and radiating elements of the base station antennas. The use of high power multi-channel transmitters, sensitive receivers, shared antennas, complex modulated signals and densely populated frequency bands imposes stringent requirements on the performance of printed circuits. As a consequence, the current specifications of electromagnetic compatibility and signal integrity are particularly demanding to the level of PIM distortion, e.g., -112 dBm third-order PIM (PIM3) level at 2×43 dBm continuous wave carriers is required for GSM900 base stations. In such circumstances, identification of sources and mechanisms of PIM generation in PCBs poses a major challenge of particular practical importance.

The conventional procedure for PIM characterization of PCB laminates is based on the two-port measurements of forward and reverse[1] PIM products at the input and output terminals of the microstrip lines fed by two-tone carriers, [10]–[13]. The line length in such a test represents a "black box" device-under-test (DUT) whose PIM performance is characterized by the gross PIM response of the PCB specimen whereas the origins of the measured PIM products remain unknown.

Mapping PIM product distributions in printed circuits has alternatively been used for *in-situ* detecting and locating the PIM sources [14]–[17]. The groundwork for this approach has been laid by the works on near-field probing of localized PIM sources in printed antennas, [16], and by microwave imaging of PIM products on the reflector antennas, [17]. The latter dedicated test setups, designed for the particular antenna applications, have been primarily used for detection of the localized PIM sources. Another setup, proposed in [14] by the authors, has been adapted for mapping PIM product distributions in printed lines and is used in this work for the study of the PIM generation mechanisms in printed circuits.

In this paper, the phenomenology of PIM production in the microstrip lines is investigated with the aid of near-field probing of PIM products. The presented results of the targeted experiments are aimed at identification of the specific features of PIM production and provide insight into the mechanisms of PIM generation through the four-wave mixing process in printed lines with weak nonlinearities. The effects of nonlinear scattering by the non-reflecting nonlinear inclusions on the PIM production are directly demonstrated for the first time.

This paper is organized as follows. The near-field probing setup is briefly described in Section II. In Section III, the results of PIM mapping are presented for the uniform microstrip lines, and for the lines containing discontinuities and nonlinear inclusions. The mechanisms of PIM generation in printed circuits are discussed in Section IV on the basis of the obtained experimental results. The major findings and suggestions on PIM mitigation are summarized in Section V.

Manuscript received April 28, 2008; revised August 03, 2008. First published November 18, 2008; current version published December 05, 2008. This work was supported by the U.K. Engineering and Physical Science Research Council under Grant EP/C00065X/1.

The authors are with the Institute of Electronics, Communications and Information Technology, Queen's University of Belfast, Belfast BT3 9DT, U.K. (e-mail: a.shitvov@qub.ac.uk; d.zelenchuk@qub.ac.uk; a.schuchinsky@qub.ac.uk; v.fusco@ecit.qub.ac.uk).

Color versions of one or more of the figures in this paper are available online at http://ieeexplore.ieee.org.

Digital Object Identifier 10.1109/TMTT.2008.2007136

[1]Generated by two-tone carriers, the forward PIM products travel in the same direction as the carriers and are measured at the line output. Reverse PIM products travel in the direction opposite to the carriers and are measured at the line input port.

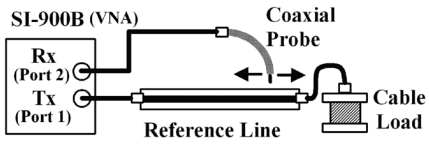

Fig. 1. Schematic of the test arrangement for near-field probing.

II. Test Setup

The measurement setup shown schematically in Fig. 1 is based upon the Summitek Instruments SI-900B PIM analyzer [18], which is used here for both conventional two-port forward/reverse tests of PIM products and near-field probing. The transmitter port of the PIM analyzer is connected to the input of the tested line and supplies the carriers in both configurations, while the receiver port is connected either: 1) to output of the tested line, when measuring the gross forward PIM response of the specimen or 2) to a probe, when measuring near-field of PIM products on the line terminated in the matched load.

The low PIM cable load had the residual reverse PIM3 level below -134 dBm at PIM3 frequency of 910 MHz, and carriers of frequencies 935 MHz and 960 MHz at 2×43 dBm. Residual forward PIM3 level of the PIM analyzer with the cables was below -125 dBm at the same power rate of the carriers.

The capacitive E-field probes have been used for mapping PIM3 product distributions on the printed microstrip lines. The analysis of several probe configurations, carried out in [14], has shown that the probes with weak coupling less than -30 dB caused minor perturbation of the near field in the printed line and had negligible effect on the measured PIM response. All the results of PIM3 mapping presented in the paper have been obtained with the probe made of a semi-rigid coaxial cable of diameter 6.35 mm. The probe tip was formed by the inner conductor of diameter 1.58 mm protruding from the shield for 6 mm and covered by the 6.7 mm long polyethylene sleeve. The probe was placed vertically and its insulating cover consistently maintained the 0.7 mm gap between the board surface and the tip, which provided the coupling -32 ± 1.5 dB.

The actual PIM3 level $P_{\mathrm{IM3}}(x)$ at point x on the line has been retrieved from the data of near-field probing as follows:

$$P_{\mathrm{IM3}}(x) = P_{\mathrm{probe}}(x) - P_{cpl}$$

where $P_{\mathrm{probe}}(x)$ is the probe reading of PIM3 magnitude at observation point x, and $P_{cpl} = \langle |S_{21}| \rangle$ was obtained by averaging the linear S-parameters measured along the line.

Negligible contribution of the probe itself to the PIM3 level has been verified by comparison of the forward PIM3 magnitude (-80.1 dBm) measured on the reference line in the two-port transmission test with the results of near-field probing at the strip output port (-78.9 dBm).

To lower the noise floor and suppress the effect of external sources, all the measurements have been performed in the screened anechoic chamber. Further details of the test setup for near-field probing of PIM products were reported in [14].

III. Near-Field Mapping of PIM Products

Mapping of PIM product distributions on printed lines has enabled us to explore the mechanisms and sources of PIM generation, and the effects of the extrinsic factors on PIM production, including the test line matching, interference with external sources, etc. The distinctive features of the distributed and localized PIM generation observed with the aid of the near-field probing are discussed here to provide insight in the phenomenology of PIM production in the printed circuits.

A. Mapping of Distributed PIM3 Products

As reported in the earlier study [12], the gross forward PIM3 level grows with the microstrip line length. Such a cumulative intensification of the forward PIM3 products had been observed in the two-port forward/reverse measurements on the lines of different lengths and was attributed to the distributed sources of PIM generation. This concept underlies the nonlinear transmission line (NTL) model of PIM generation in printed lines, [19], which predicts cumulative growth of PIM level with length of the microstrip lines. Although the two-port forward/reverse measurements of PIM3 products on printed lines of different lengths demonstrate the cumulative growth, they do not constitute the direct evidences of distributed nature of PIM generation. Alternatively, the near-field mapping of the spatial distribution of PIM products along the printed traces could shed the light on the process of PIM generation and conclusively justify the assumptions of the NTL model.

The PIM3 products have been mapped on the reference 50 Ω straight uniform microstrip line (Sample 1) of width 1.87 mm and length 915 mm fabricated on the Taconic TLG-30 substrate of thickness 0.76 mm. The results in Fig. 2 show that PIM3 magnitude grows along the line, and such profile fully agrees with the predictions of the NTL model. However, in contrast to the monotonic increase of the gross forward PIM3 level observed in the two-port measurements [12], the mapped PIM3 distribution has periodic ripples. The cause of this discrepancy is understandable if we note that in the two-port tests, magnitudes of the forward and reverse PIM products are measured separately, whereas the near-field probing gives the gross local PIM level at each observation point. This subtle feature is illustrated in Fig. 3, where the simulated PIM3 distribution on a microstrip line of the length 915 mm is juxtaposed with the forward PIM3 magnitude calculated at the output ports of the lines with the length varying from 10 mm to 915 mm. Although the local and forward PIM3 levels are equal at the output of the 915 mm long line, the local PIM3 profile has regular ripples, which are caused by interference of the PIM3 products traveling in forward and backward directions as discussed in Section IV. It is important to note that the ripples exist on the perfectly matched lines but their magnitude increases with input/output mismatch, cf. [19], [20]. This effect is confirmed by full agreement of the measurement results with the simulations of the 50 Ω line terminated in the 48 Ω source and load impedances, as shown in Fig. 2.

To further elucidate the process of PIM generation, PIM3 products have been mapped on the two identical microstrip lines: Sample 1 and its replica (Sample 2) fabricated on the

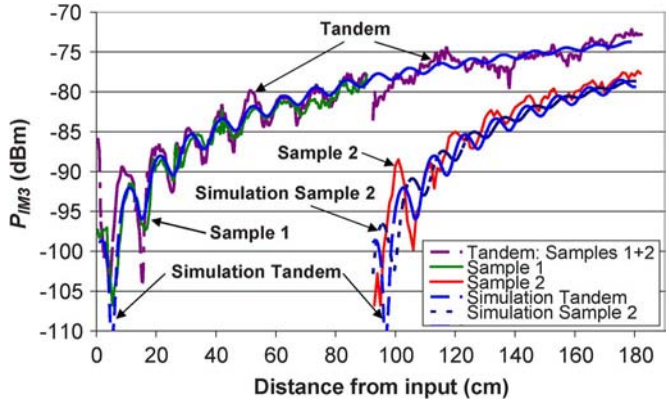

Fig. 2. PIM3 product distributions on the identical microstrip lines, Sample 1 and Sample 2, simulated and measured separately and in cascaded arrangement at PIM3 frequency of 910 MHz and carriers' power of 2 × 44 dBm. Both curves "Simulation Tandem" are identical, but plotted with 915 mm offset from each other. Measurement data from [14].

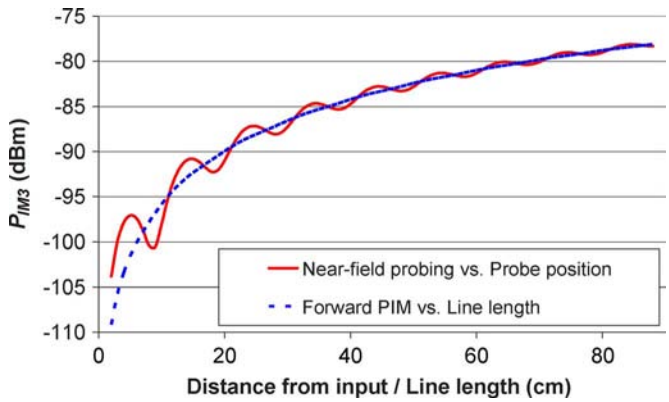

Fig. 3. Simulated PIM3 product distribution on a microstrip line of length 915 mm (emulated near-field probing) and forward PIM3 response at the output of the lines with lengths varying from 10 to 915 mm (emulated two-port test). The calculations are performed at PIM3 frequency of 910 MHz, carrier frequencies of 935 and 960 MHz, and power of 2 × 43 dBm.

same board and connected in series via a 1.5 m long PIM-certified coaxial cable. The profiles of PIM3 distributions, measured and simulated with the aid of the NTL model [19], are shown in Fig. 2. The model parameters, such as the nonlinear resistivity and port reflection coefficients of microstrip line, have been retrieved from the PIM3 mapping of Sample 1 terminated in the cable load. Then these parameters have been applied to simulation of PIM3 distribution on Sample 2 and on the whole tandem assembly. As one can observe in Fig. 2, the NTL simulations are in an excellent agreement with the measured PIM3 patterns on both the individual samples and their cascaded assembly. It is necessary to note that the interconnecting cable, microstrip launchers and Sample 2 in the cascaded arrangement affect PIM3 product distribution on Sample 1. This effect can be observed also in the simulated PIM3 profiles on the tandem and Sample 1, which are slightly offset from each other in Fig. 2. Indeed, since the input impedance of the terminated Sample 2 is not exactly 50 Ω, it causes an additional mismatch and deeper ripples in PIM3 product distribution on Sample 1, especially close to its input. Also, the reflection and additional phase shift of carriers in the cable connecting the cascaded lines cause a

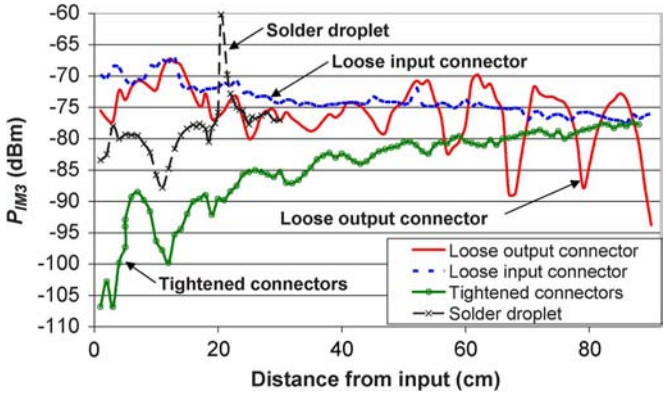

Fig. 4. PIM3 product distributions on Sample 2 mapped at PIM3 frequency of 910 MHz and carriers' power of 2 × 44 dBm.

discontinuity in the experimental PIM3 distribution at distance of 915 mm from the tandem input (Fig. 2), where the curves for Sample 1 and Sample 2 are joined in.

Thus, the presented results of PIM3 mapping provide conclusive evidences of the distributed nature of PIM3 generation in the tested microstrip lines.

B. Mapping of Localized PIM Sources

In contrast to the distributed PIM sources, the localized nonlinearities are often accompanied by the circuit discontinuities, which can cause additional linear scattering and interference. This leads to formation of the standing waves of carriers, which may further distort PIM distributions. Therefore, it is important to identify and separate the effects of linear and nonlinear scattering in printed lines. At the same time, the latter phenomenon of purely nonlinear scattering by small nonlinear inclusions is of particular interest because it is inherently related to the distributed PIM production in the printed lines as detailed in Section IV. In order to investigate the properties of PIM generation by the localized sources of different types in printed circuits, PIM products have been mapped on microstrip lines with loose connectors and lumped nonlinear inclusions, such as a solder droplet, a ferrite disk and graphite pencil marks.

PIM3 product distributions on the microstrip line, Sample 2, with loose input and output connectors are shown in Fig. 4. Since a loose connector produces both a linear discontinuity and a PIM source, the distributed and locally generated PIM3 products interfere. However, the PIM patterns created by the input and output connectors distinctively differ. The PIM3 products generated by the loose input connector significantly increase PIM3 level at line input port. Small undulations due to interference with the reverse PIM3 products generated by the distributed sources can be observed at the distance of order of a wavelength λ_P ($\lambda_P = 21.2$ cm in the microstrip line at the PIM3 frequency of 910 MHz) from the line input. However, they gradually decay toward the line output, where the PIM3 level is predominantly determined by the forward PIM3 products and becomes nearly equal to that on the line with the tightened connectors. This pattern of the PIM3 products distribution is associated with the distributed PIM generation as further discussed in Section IV.

The PIM3 distribution on the line with the loose output connector significantly differs from the previous case due to the standing wave of the carriers trapped on the line. This affects the PIM3 profile not only at the line output but also at the input port, where the PIM products reflected from the discontinuity interfere with the reverse PIM products generated by the distributed sources. At the output port, magnitude of the PIM3 undulations considerably increases as the result of interference between the forward PIM products from the distributed sources, which grow toward the loose output connector and become commensurate with the PIM produced by the localized source. It is also noteworthy that the near-field probing in the port vicinities correlate fairly well with the two-port PIM3 measurements when the loose connectors are at the following locations.

- At the input: −76 dBm (probed at 90 cm from the input port) versus −77.4 dBm (forward).
- At the load: −79.2 dBm (probed at 1 cm from the input port) versus −75.5 dBm (reverse).

In contrast to the loose connectors, a lumped nonlinearity created by the solder droplet of 60/40 tin/lead solder (about 1 mm in diameter) does not inflict considerable linear scattering and interference of the PIM products. Placed at the strip center of the matched microstrip line of Sample 2 at distance of 21 cm (nearly equal to λ_P) from the line input, the droplet causes a sharp spike of PIM3 level in its vicinity (see Fig. 4). Away from the droplet, however, the PIM3 level rapidly falls and remains about 10 dB above the PIM3 level in the unperturbed microstrip line.

To further investigate the effects of the nonlinear scattering by localized PIM sources, PIM3 products have been mapped on the lines with the nonlinear inclusions, which had negligible effect on the linear S-parameters. A ferrite disk of diameter 20 mm and thickness 2 mm was placed beside the strip edge of the microstrip line of Sample 1, as illustrated in Fig. 5(a). In this case, the disk had no direct contact with the conductor trace and was weakly coupled via the strip fringing field. The linear S-parameter measurements have shown no discernable effect of the disk on the microstrip line response, while the disk is readily detectable via the PIM3 product distributions [see Fig. 5(b)].

Uncertainty of mapping PIM3 products has been assessed first by repeating twice the near-field probing when the ferrite disk was located at $D_x = 16$ cm from the line input and $D_y = 1$ mm from the strip edge (probe was moved along the strip center line with 10 mm step and 5 mm offset between the two passes). The corresponding plots of PIM3 distributions in Fig. 5(b) show fairly consistent patterns.

Impact of the disk position on PIM response was explored next. As demonstrated in Fig. 5(b), interference of PIM3 products generated by the ferrite disk and the printed line itself alters the overall PIM response. Notably, the disk placed at distance of $D_x = 21$ cm $\approx \lambda_P$ from the line input produces a sharp spike of PIM3 level similarly to the solder droplet. Alternatively, when the disk is placed at $D_x = 16$ cm $\approx 3\lambda_P/4$ and $D_x = 31.5$ cm $\approx 3\lambda_P/2$, deep notches in PIM3 distributions arise between the disk and line input. These observations suggest that PIM3 products generated by the distributed sources in the line and by the nonlinear ferrite disk strongly interfere with each other. The resulting PIM3 product distributions in the line vary with the disk position in accordance with the conditions of

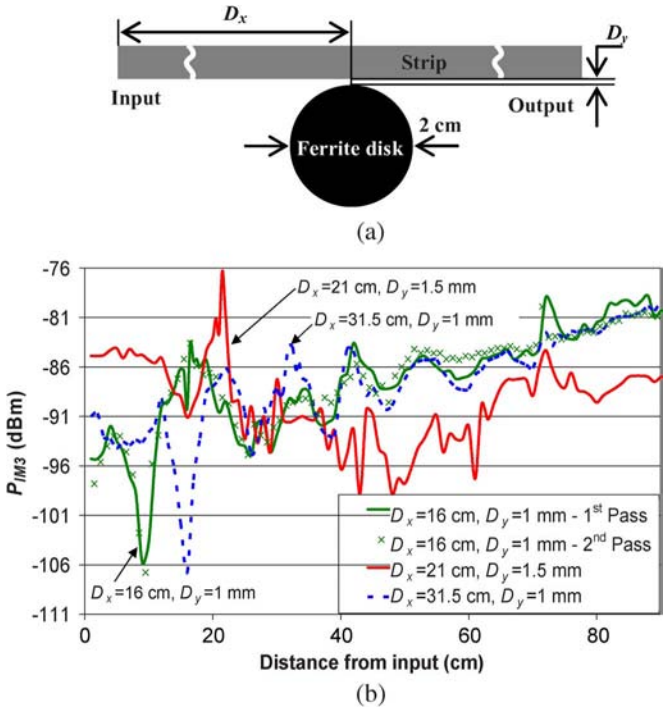

Fig. 5. PIM3 product distributions on sample 1 with the ferrite disk placed near the strip edge (PIM3 frequency 910 MHz, carriers' power 2 × 43 dBm).

phase synchronism (see Section IV) between the PIM3 products generated by the distributed and lumped nonlinearities.

To gain deeper insight into the effect of nonlinear scattering in printed lines, a lumped nonlinearity was created in the microstrip line (Sample 3) by a small graphite pencil mark drawn on the top of the strip conductor. The Sample 3 was fabricated on the low-PIM Taconic TLX-9 laminate of thickness 1.58 mm. The microstrip trace comprises a section of 522 mm long strip of width 13.46 mm between the tapered line sections providing the matching to the 50 Ω input/output microstrip lines of width 4.32 mm. The forward and reverse PIM3 products measured on Sample 3 were below the instrument residual level of −125 dBm. A small pencil mark of size 3.5×1 mm^2, representing the localized nonlinearity, was placed near the strip edge in the middle of the wide central section. In linear regime, neither the S-parameter measurements nor the near-field probing have shown a discernable effect of the pencil mark at PIM3 frequency of 910 MHz.

A surface map of PIM3 products generated by the pencil mark (centered at the origin) is shown in Fig. 6(a). PIM3 profiles along the trace center line and the edges (marked in Fig. 6(a) by white horizontal lines at 0 and 13.46 mm) are displayed in Fig. 6(b). It is noteworthy in Fig. 6(b) that away from the pencil mark, the PIM3 level at the trace center is about 5 dB higher than at the edges. The latter effect is attributed to the stronger vertical electric field at the strip center than at the edges. Inspection of Fig. 6 shows that the pencil mark not only produces a sharp local spike, like the solder droplet in Fig. 4, but also substantially increases the base PIM3 level on the line. Furthermore it was observed that PIM3 products, emanated by the pencil mark, nearly equally contribute to the gross forward and reverse PIM3

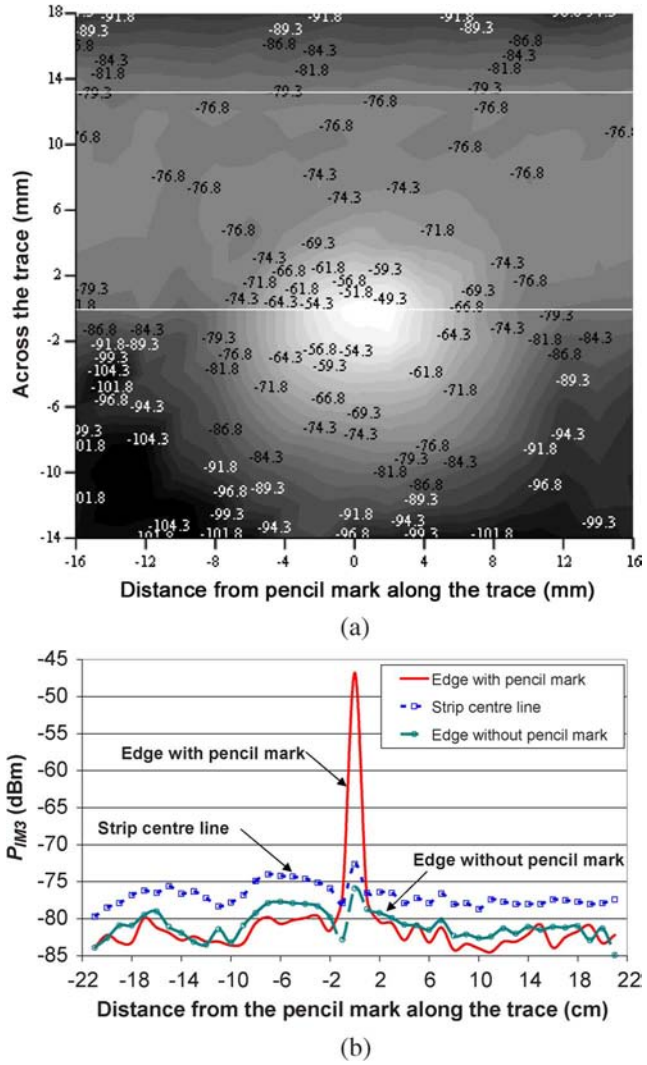

Fig. 6. PIM3 product distributions on Sample 3 with the pencil mark acting as a localized nonlinearity (centered at the origin) at PIM3 frequency of 910 MHz and carriers' power 2 × 43 dBm. (a) Surface map of PIM3 products about the pencil mark (the trace edges are marked by the white horizontal lines). (b) PIM3 product profiles along the strip edges and the center line.

levels of −77.8 and −78 dBm, respectively, measured at the line terminals.

The most remarkable feature of the PIM3 pattern in Fig. 6(a) is that the pencil mark acts as an isotropic source as illustrated by the nearly concentric contour lines. The high PIM3 level in the close proximity of the localized nonlinearity indicates that considerable reactive power is engaged in the process of nonlinear scattering and conversion of carriers into the PIM products. While the reactive power is confined to the lumped nonlinearity, only its small portion is coupled to the traveling waves on the line. Therefore, the PIM level measured at the printed line terminals is substantially lower than that at the PIM source.

The effect of the lumped nonlinearities on PIM3 product interference in printed lines has been investigated on a microstrip line (Sample 4) with two pencil marks, Fig. 7. Sample 4 is a straight uniform 50 Ω microstrip line of length 917 mm fabricated on the low-PIM Taconic TLX-9 laminate. The initial two-port tests of Sample 4 without the marks at PIM3 frequency

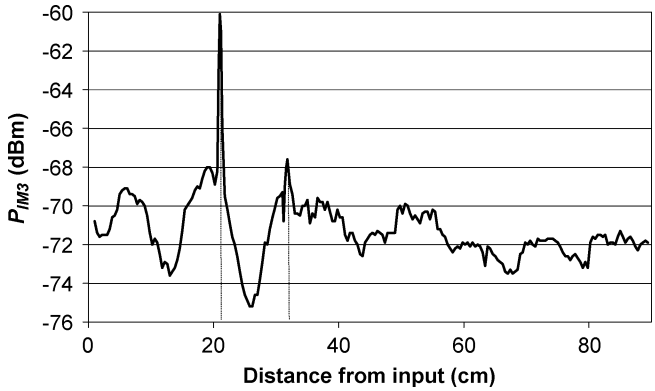

Fig. 7. PIM3 product distributions on Sample 4 with two pencil marks drawn across the trace at 21 cm and 31.5 cm from the line input and acting as the localized nonlinearities (at the locations of two spikes on the plot). PIM3 frequency is 910 MHz and carriers' power is 2 × 43 dBm.

of 910 MHz and carriers' power 2 × 43 dBm have shown the forward and reverse PIM3 levels at −113 dBm and −119 dBm, respectively. As the two 0.2 mm wide pencil marks were drawn across the strip at the distances of 21 and 31.5 cm from the input, both forward and reverse PIM3 levels grew to −77.1 and −77.5 dBm, respectively.

The main results of the observations of PIM3 production on Sample 4 with two pencil marks (Fig. 7) can be summarized as follows.

- Sharp spikes on PIM3 profiles occur in the vicinities of both pencil marks.
- The pencil marks, undetectable in linear regime, increase the base PIM3 level for more than 40 dB, thus obscuring the contribution of the distributed sources.
- The interference pattern exists in the PIM3 distribution between the line input and the second pencil mark at distance of 31.5 cm from the input. This observation is in qualitative agreement with the experimental results in [16], which were solely attributed to the effect of the input/output matching. However, as illustrated by the results of our study, the latter interpretation is valid only when contribution of the distributed PIM3 sources is negligible as compared with the PIM3 products generated by the lumped nonlinearities.
- Average PIM3 level gradually decreases toward the line output due to dissipation of PIM3 products generated by the localized sources (pencil marks).

Thus, the presented results of mapping the PIM product distributions on printed lines have exposed the fundamental properties of PIM3 generation by the distributed and localized sources. The unique signatures of the PIM products can be used for identification of the dominant PIM generation mechanism and for location of the lumped sources in the printed lines.

IV. Mechanisms of PIM Generation

As demonstrated in Section III, PIM3 products in printed lines originating from the distributed and localized sources exhibit substantially different behaviour. On the other hand, comparison of the PIM3 profiles generated by the localized sources of three different types: the solder droplet (Fig. 4), ferrite disk

(Fig. 5) and pencil mark (Fig. 6), shows similarity of their patterns. Namely, irrespectively of the nonlinearity type, contact (droplet and pencil mark) or contactless (ferrite disk), considerable reactive power is confined to the proximity of the nonlinear lumped inclusions where the carriers undergo conversion into PIM products. The localized nonlinearities act here as the isotropic point sources irradiating PIM products into the printed line as illustrated in Fig. 6 for the pencil mark.

In contrast to the localized PIM sources, the individual microscopic nonlinearities in the printed lines could not be detected directly in our near-field probing setup. Nevertheless, the mappings of PIM3 products of the localized sources provide invaluable insight into the mechanisms of distributed PIM3 production. Indeed, considering a printed line as a continuum of localized sources, the processes of distributed PIM3 generation can be comprehensively described in terms of the nonlinear scattering by the point nonlinearities [cf. Fig. 6(a)] and the phase synchronism, or phase matching, in a four-wave mixing process, see [21].

Let us consider PIM3 products in the matched lossless NTL at frequency $f_P = 2f_1 - f_2$, which result from scattering the two-tone carriers of frequencies f_1 and f_2 at a point nonlinearity. The phase difference between the PIM3 products, generated by two identical point sources at x_1 and x_2 ($x_2 > x_1$) and traveling in the forward direction, equals $\Delta_f(L) = (2k_1 - k_2)L - k_P L$, where $L = x_2 - x_1$, and $k_{1,2,P}$ are the wave numbers of the respective tones. When dispersion in the microstrip line is negligible, $\Delta_f(L) = 0$ for any L. Thus the forward PIM3 products, generated at each point x, constructively interfere, and the cumulative intensification of PIM3 occurs at the line output.

If $\Delta_f(L) \neq 0$, for instance due to dispersion, the PIM3 products generated at a pair of points x_1 and x_2, spaced apart for distance L_{Sf}, may accrue a phase shift equal to π, i.e. $\Delta_f(L_{Sf}) = \pi$. The length L_{Sf} is known as the coherence distance [21]. In such a dispersive transmission line, the output forward PIM3 level increases with L and reaches the maximum at L equal to L_{Sf} or odd multiples of L_{Sf}, see (A2) in Appendix. This maximum is the result of constructive interference of the PIM3 products generated by the sources located between points x_1 and x_2 ($|x_2 - x_1| < L_{Sf}$). In the lines longer than L_{Sf}, forward PIM3 level decreases and, at L equal to $2L_{Sf}$, the output forward PIM3 products vanish, cf. (A2). This occurs because the length $2L_{Sf}$ always contains a pair of point sources at x_1 and $x_2 = x_1 + L_{Sf}$ whose PIM3 products destructively interfere at the output. In the ideal non-dispersive transmission lines $L_{Sf} = \infty$, so that the output forward PIM level monotonically grows with the line length. However, in practice the growth of PIM3 products is capped by attenuation of carriers. Therefore the actual PIM level always decays beyond certain line length, which is determined by the propagation loss, [22].

The PIM3 products, traveling from the point sources at x_1 and x_2 in the reverse direction, have the phase difference $\Delta_r(L) = (2k_1 - k_2)L + k_P L$. Notably, $\Delta_r(L) \neq 0$ even in the nondispersive line, and the coherence distance L_{Sr}, corresponding to $\Delta_r(L_{Sr}) = \pi$, equals $L_{Sr} = \lambda_P/4$, where λ_P is the wavelength at PIM3 frequency. Therefore, the distribution of reverse PIM3 products has undulations with the troughs and humps offset from each other for the distance L_{Sr}, cf. (A2). The reverse PIM3 level measured at the line input varies with the line length even in the ideal non-dispersive matched transmission line. Furthermore, the magnitude of the reverse PIM3 products at the line input cannot exceed the level generated by the line section of the length L_{Sr}. This upper bound arises because on the lines longer than L_{Sr}, the contributions of the sources located at x_1 and $x_2 = x_1 + L_{Sr}$ are annihilated. The latter effect has been observed in the two-port PIM3 measurements of the microstrip lines and is also known in nonlinear optics [21]. It is important to note that the existence of the finite coherence distance L_{Sr} suggests a means for mitigating reverse PIM3 level at the input of microstrip components by choosing the line length close to multiples of $2L_{Sr}$.

The concept of phase synchronism in the four-wave mixing process also provides a consistent interpretation of the ripples observed in the PIM3 product distributions in Figs. 2 and 3. Indeed, while of the forward PIM3 level monotonically grows along the line, the reverse PIM3 level alternates with the periodicity $2L_{Sr} = \lambda_P/2$. Therefore, PIM3 distributions along the line formed by the superposition of the forward and reversed PIM3 products exhibit undulations.

As mentioned earlier, the reverse PIM3 level varies with the line length. This proved to be the cause of the slight offset between the positions of troughs/humps observed in the simulated PIM distributions on the two lines of lengths $L_1 = 915$ mm and $L_2 = 1830$ mm (Fig. 2). Namely, the contributions of forward PIM3 products to the gross PIM3 level at any point $x_1 < L_1$ are equal on both lines, whereas the contribution of the reverse PIM products is determined by the distance from the output terminal, which is different for the single line and the tandem arrangement. Indeed, unless the length difference equals multiples of $\lambda_P/2$, or $2L_{Sr}$ at PIM3 frequency, the PIM3 distributions on the two specimens are offset from each other.

V. Conclusion

The mechanisms of PIM in printed lines have been explored with the aid of mapping PIM products generated by the two-tone carrier waves traveling in homogeneous microstrip lines and in the lines with nonlinear inclusions. Near-field probing setup based upon the commercial PIM analyzer and the specially designed specimens of microstrip lines have been employed for investigation of the PIM production processes in PCB materials and printed lines with localized sources. Accuracy and reliability of the near-field probing of PIM products on printed lines have been confirmed by the simulations based on the NTL model and by the two-port forward/reverse PIM measurements.

The presented results provide the direct experimental evidences of cumulative growth of PIM products in the matched uniform microstrip lines and explicitly demonstrate the patterns of PIM products created by the localized nonlinearities of the size smaller than $0.02\lambda_P$ in the test lines. It is shown experimentally that the localized nonlinearities, which are undetectable in the linear regime, act as the isotropic nonlinear sources emanating PIM products nearly omni-directionally. The measurement results demonstrate that regardless of the

nonlinearity type, contact (droplet and pencil mark) or contactless (ferrite disk), the reactive power is confined to the lumped inclusions, where the carriers undergo conversion into the PIM products. The patterns of PIM product near these localized sources have revealed the fundamental role of the nonlinear scattering and the four-wave mixing process in distributed PIM production.

The presented experimental results indicate that nonlinear scattering of the traveling waves of carriers by weak distributed nonlinearities is the primary cause of PIM production in printed lines. The distributed nature of the PIM generation in microstrip lines has been conclusively demonstrated and described in terms of phase synchronism in the four-wave mixing process. The proposed phenomenology of distributed PIM production by the continuum of point sources proved to be fully consistent with the experimental observations of PIM3 products on the matched and mismatched microstrip lines. It has been shown that the standing waves of carriers created by linear discontinuities distort the PIM product patterns and alter the PIM performance of printed lines.

The concept of phase synchronism in the four-wave mixing process provides a consistent interpretation of the cumulative growth of forward PIM products and the existence of the upper bound for the reverse PIM3 level. The origins of ripples in the PIM3 product distributions have also been explained. The presented results suggest that the reverse PIM3 level at the microstrip line input can be mitigated when the line length is close to multiples of the double coherence distance $(2L_{Sr})$.

APPENDIX

Complex amplitudes of PIM3 waves $A_{f,r}(x)\exp(\pm ik_P x)$ traveling in forward and backward directions in a lossless weakly nonlinear transmission line can be obtained following the approach developed in [21]

$$\frac{dA_{f,r}(x)}{dx}\exp(\pm ik_P x) = cA_1^2A_2^*\exp\left(i(2k_1-k_2)x\right) \quad \text{(A1)}$$

where c is a mixing coefficient and $A_{1,2}$ are the carriers' amplitudes. Having integrated (A1) and fulfilling the boundary conditions of $A_f(0)=0$ and $A_r(L)=0$, one finds magnitudes of the forward and reverse PIM3 products at the output and input of the line of length L, respectively,

$$\begin{aligned}|A_f(L)| &= \left|cA_1^2A_2^*\right| L\left|2\sin\left(\frac{\Delta_f(L)}{2}\right)\Big/\Delta_f(L)\right| \\ |A_r(0)| &= \left|cA_1^2A_2^*\right| L\left|2\sin\left(\frac{\Delta_r(L)}{2}\right)\Big/\Delta_r(L)\right| \quad \text{(A2)}\end{aligned}$$

where $\Delta_{f,r}(L)=(2k_1-k_2)L\mp k_P L$ are defined in Section IV. It immediately follows from (A2) that forward PIM3 level monotonically grows with L at $\Delta_f(L)=0$ (cumulative effect) and maxima of $|A_{f,r}(L)|$ occur at $\Delta_{f,r}(L)=\pi$.

ACKNOWLEDGMENT

The authors are grateful to Taconic Advanced Dielectric Division Ltd., Trackwise Designs Ltd., PCTEL Inc., and Castle Microwave Ltd. for providing the test samples and measurement facilities. Special thanks go to J. Francey for his continuous support and to N. Carroll for his help with the measurements. The authors also wish to acknowledge the advice provided by Dr. D. Linton and Dr. O. Malyuskin, both with Queen's University of Belfast, Belfast, U.K., over the period of this study.

REFERENCES

[1] M. T. Abuelma'atti, "Prediction of passive intermodulation arising from corrosion," *Proc. Inst. Elect. Eng.—Sci., Meas., Technol.*, vol. 150, no. 1, pp. 30–34, Jan. 2003.

[2] W. D. Watson, "The measurement, detection, location and suppression of external non-linearities which affect radio systems," in *Proc. Electromagn. Compat. Conf.*, Southampton, U.K., Sep. 1980, pp. 1–10.

[3] C. Vicente, D. Wolk, H. L. Hartnagel, B. Gimeno, V. E. Boria, and D. Raboso, "Experimental analysis of passive intermodulation at waveguide flange bolted connections," *IEEE Trans. Microw. Theory Tech.*, vol. 55, no. 5, pp. 1018–1028, May 2007.

[4] G. Macchiarella, G. B. Stracca, and L. Miglioli, "Experimental study of passive intermodulation in coaxial cavities for cellular base stations duplexers," in *Proc. 34th Eur. Microw. Conf.*, Amsterdam, The Netherlands, Oct. 2004, pp. 981–984.

[5] K. G. Gard, M. B. Steer, and J. R. Wilkerson, "Electro-thermal passive intermodulation distortion in microwave attenuators," in *Proc. 36th Eur. Microw. Conf.*, Manchester, U.K., Sep. 2006, pp. 157–160.

[6] A. K. Brown, "Passive intermodulation products in antennas-an overview," in *Proc. IEE Passive Intermodulation Products in Antennas and Related Structures Colloq.*, London, U.K., Jun. 1989, pp. 1/1–1/3.

[7] A. P. Foord and A. D. Rawlins, "A study of passive intermodulation interference in space RF hardware," Univ. Kent, Canterbury, U.K., ESTEC Tech. Rep. 111036, May 1992.

[8] J. Russer, A. Ramachandran, A. Cangellaris, and P. Russer, "Phenomenological modeling of passive intermodulation (PIM) due to electron tunneling at metallic contacts," in *IEEE MTT-S Int. Microw. Symp. Dig.*, San Francisco, Jun. 2006, pp. 1129–1132.

[9] Z. Shi-quan and G. De-biao, "The generation mechanism and analysis of passive intermodulation in metallic contacts," in *Proc. 4th Asia–Pacific Environmental Electromagn. Conf.*, Dalian, China, Aug. 2006, pp. 546–549.

[10] N. Kuga and T. Takao, "Passive intermodulation evaluation of printed circuit board by using 50 Ω microstrip line," in *Proc. Asia–Pacific Microw. Conf.*, New Delhi, India, Dec. 2004, pp. 1008–1009.

[11] J. V. S. Perez, F. G. Romero, D. Rönnow, A. Söderbärg, and T. Olsson, "A micro-strip passive inter-modulation test set-up; comparison of leaded and lead-free solders and conductor finishing," in *Proc. Int. Multipactor, Corona, Passive Intermodulation in Space RF Hardware Workshop*, Noordwijk, The Netherlands, Sep. 2005, pp. 215–222.

[12] A. G. Schuchinsky, J. Francey, and V. F. Fusco, "Distributed sources of passive intermodulation on printed lines," in *Proc. IEEE Int. AP-S Symp.*, Jul. 2005, vol. 4B, pp. 447–450.

[13] A. P. Shitvov, D. E. Zelenchuk, A. G. Schuchinsky, and V. F. Fusco, "Passive intermodulation in printed lines: Effects of trace dimensions and substrate," *IET Microw. Antennas Propag.*, to be published.

[14] A. P. Shitvov, D. E. Zelenchuk, A. G. Schuchinsky, V. F. Fusco, and N. Buchanan, "Mapping of passive intermodulation products on microstrip lines," in *IEEE MTT-S Int. Microw. Symp. Dig.*, Atlanta, GA, Jun. 2008, THP2H-02.

[15] A. P. Shitvov, D. E. Zelenchuk, and A. G. Schuchinsky, "Experimental observations of distributed nonlinearity in printed lines," in *Proc. 14th Int. Microw. Opt. Appl. Novel Physical Phenomena Student Seminar*, Belfast, U.K., Aug. 2007, pp. 70–73.

[16] S. Hienonen and A. V. Raisanen, "Passive intermodulation near-field measurements on microstrip lines," in *Proc. 34th Eur. Microw. Conf.*, Amsterdam, The Netherlands, Oct. 2004, pp. 1041–1044.

[17] P. L. Aspden, A. P. Anderson, and J. C. Benett, "Evaluation of the intermodulation product performance of reflector antennas and related structures by microwave imaging," in *IEE Passive Intermodulation Products in Antennas and Related Structures Colloq. Dig.*, 1989, pp. 853–858, no. 94.

[18] *"Passive IM Distortion Analyzer: Operating and Maintenance Manual,"* Summitek Instrum., Englewood, CO, Jun. 2001, Rev. B, no. 1902000.

[19] D. E. Zelenchuk, A. P. Shitvov, A. G. Schuchinsky, and T. Olsson, "Passive intermodulation on microstrip lines," in *Proc. 37th Eur. Microw. Conf.*, Munich, Germany, Oct. 2007, pp. 396–399.

[20] D. E. Zelenchuk, A. P. Shitvov, and A. G. Schuchinsky, "Effect of matching on passive intermodulation in transmission lines with distributed nonlinear resistance," in *Proc. Int. URSI Commission B—Electromagn. Theory Symp.*, Ottawa, ON, Canada, Jul. 2007, R19–39.
[21] N. Bloembergen, *Nonlinear Optics*. New York: Benjamin, 1965.
[22] B. A. Auld, M. Didomenico, Jr., and R. H. Pantell, "Traveling-wave harmonic generation along nonlinear transmission lines," *J. Appl. Phys.*, vol. 33, pp. 3537–3545, Dec. 1962.

Aleksey P. Shitvov received the Diploma Specialist degree in semiconductor devices and microelectronics from Nizhny Novgorod State University (NNSU), Nizhny Novgorod, Russia, in 1995, and is currently working toward the Ph.D. degree at Queen's University of Belfast, Belfast, U.K.

From 2000 to 2004, he was a Research Assistant with the Department of Electronics, NNSU, where he was involved with the design and simulation of the devices based on surface acoustic waves. His current research is focused on PIM phenomena in printed lines and PCB laminates. His research interests include experimental design and measurement of PIM products and phenomenology of nonlinear effects in PCBs and transmission lines.

Dmitry E. Zelenchuk (S'02–M'05) received the B.Sc. and M.Sc. degrees in physics and Ph.D. in radiophysics from Rostov State University, Rostov-on-Don, Russia, in 1999, 2001, and 2004, respectively.

From 2003 to 2005, he was a Lecturer with the Department of Applied Electrodynamics and Computer Modelling, Rostov State University. He is currently a Research Fellow with the Queen's University of Belfast, Belfast, U.K. He has authored or coauthored over 40 journal and conference papers. His research interests include numerical and analytical methods for the problems of electromagnetic field theory, numerical modeling of frequency-selective surfaces, linear and nonlinear phenomena in planar circuits and antennas, including PIM, and various physical phenomena of plasmonic nanostructures.

Dr. Zelenchuk was the recipient of the 2001 Medal of Ministry of Education of the Russian Federation for the Best Scientific Student Paper.

Alexander G. Schuchinsky (M'97–SM'05) received the M.Sc. degree in radiophysics from Rostov State University, Rostov-on-Don, Russia, in 1973, and the Ph.D. degree in radiophysics from the Leningrad Electrotechnical Institute, Leningrad, Russia, in 1983. He was awarded the title of Senior Research Scientist in 1988.

From 1973 to 1994, he was with the Microwave Electrodynamics Laboratory, Rostov State University, Russia, where he held the position of Leading Scientist. From 1994 to 2002, he was with Deltec-Telesystems New Zealand. Since 2002, he has been a Reader with the School of Electronics, Electrical Engineering and Computer Science, Queen's University Belfast, Belfast, U.K. He has authored or coauthored over 130 papers in major journal and conference proceedings. He holds three U.S. patents. He is a member of the Editorial Board of *Metamaterials*. His current research interests include numerical–analytical and physics-based modeling techniques, microwave and optical phenomena in complex media, metamaterials, periodic structures with linear and nonlinear inclusions, electromagnetic characterization and measurements of materials, and microwave applications of novel materials.

Dr. Schuchinsky is a member of the European Physical Society. He served as a chair of the Steering Committee of the International Congress on Advanced Electromagnetic Materials in Microwaves and Optics (Metamaterials'2007).

Vincent F. Fusco (S'82–M'82–SM'96–F'04) received the Bachelors degree in electrical and electronic engineering (with first-class honors), Ph.D. degree in microwave electronics, and D.Sc. degree from the Queen's University of Belfast, Belfast, U.K., in 1979, 1982, and 2000, respectively.

Since 1995, he has held a Personal Chair in High Frequency Electronic Engineering with the Queen's University of Belfast. His research interests include nonlinear microwave circuit design and active and passive antenna techniques. The main focus for this research is in the area of wireless communications. He has pioneered many new concepts in self-tracking antenna technology. He is currently the Research Director of the High Frequency Laboratories, The Institute of Electronics, Communications and Information Technology (ECIT), Queen's University of Belfast. He is Director of the International center for Research for System on Chip and Advanced Microwireless Integration, SoCaM. He has authored or coauthored 350 scientific papers in major journals and in referred international conferences. He authored two text books. He holds several patents and has contributed invited chapters to books in the field of active antenna design and electromagnetic field computation.

Prof. Fusco is a Fellow of the Royal Academy of Engineering and the Institute of Electrical Engineers (IEE) U.K. He was the recipient of a 1986 British Telecommunications Fellowship. In 1997, he was awarded the NI Engineering Federation Trophy for outstanding industrially relevant research.